Penetration and Ricochet Phenomena in Oblique Hypervelocity Impact

William P. Schonberg*
University of Alabama, Huntsville, Alabama
and
Roy A. Taylor
NASA Marshall Space Flight Center, Huntsville, Alabama

This paper describes the results of an experimental investigation of phenomena associated with the oblique hypervelocity impact of spherical projectiles on multisheet aluminum structures. A series of equations that can be employed in the design of meteoroid and space debris protection systems for space structures is developed. These equations relate the perforation damage of a multisheet structure to parameters such as projectile size, impact velocity, and trajectory obliquity and are obtained through a regression analysis of oblique hypervelocity impact test data. These data show that the response of a multisheet structure to oblique impact is significantly different from its response to normal hypervelocity impact. It was found that obliquely incident projectiles produce ricochet debris that can severely damage panels or instrumentation located on the exterior of a space structure. Obliquity effects of high-speed impact must, therefore, be considered in the design of any structure exposed to the hazardous meteoroid and space debris environment.

Introduction

ALL spacecraft with a mission duration of more than a few days are susceptible to impacts by meteoroids and pieces of orbiting space debris. These impacts occur at high speeds and can damage flight-critical systems of a spacecraft. This damage can in turn lead to catastrophic failure of the spacecraft. Therefore, the design of a spacecraft for a long-duration mission must take into account the effects of such impacts on the spacecraft structure and on all of its exposed subsystem components such as solar arrays or instrumentation units. Until recently, meteoroid impact was better understood and believed to be more serious than the impact of orbital space debris. However, recent studies have determined that orbital debris is becoming an increasingly serious hazard to long-duration near-Earth space structures.[1-3] In certain regions of Earth orbit, the threat of orbital debris impact now exceeds the threat posed by meteoroid impact and is expected to increase.[4] It has become evident that the orbital debris problem is serious, and that the probability of collision is rising steadily. Protective systems must be developed in order to ensure the safety of a spacecraft and its occupants when encountering the space debris environment.

The design of meteoroid/space debris protection systems depends largely on the ability to predict the behavior of a variety of structural components under conditions of meteoroid or space debris impact. Forty years ago, it was suggested that "meteoroid bumpers" could be used to minimize the damage caused by the high-speed impact of meteoroids because they fragment the projectile and spread the projectile and shield debris.[5] The debris impacting the main structural wall will then be extremely small and will have little penetrating power. Since then, numerous investigations have been performed to determine the resistance of multisheet structures to hypervelocity impact [see, e.g., Refs. (6-9)] and to develop penetration criteria for such structures.[10,11]

Received Jan. 19, 1988; revision received May 31, 1988.

*Assistant Professor, Department of Mechanical Engineering. Member, AIAA.

†Chief, Laboratory Support Branch, Materials and Processes Laboratory.

In the majority of previous investigations of hypervelocity impact, the trajectories of the projectiles were normal to the surfaces of the impacted test specimens. However, it is becoming increasingly evident that most meteoroid or space debris impacts will not occur normal to the surface of a spacecraft (Fig. 2.1-4 in Ref. 12). Unfortunately, information on oblique hypervelocity impact is relatively scarce, so it is difficult to assess the severity of such impacts on a structure. Furthermore, studies of oblique impact that have been performed typically do not discuss the possibility of damage to external systems due to ricochet debris particles.[13-16]

To increase the understanding of phenomena associated with oblique hypervelocity impact, a program of research was developed to generate and analyze oblique hypervelocity impact test data. The results of this research program are presented in this paper.

After a review of the experimental procedure used in the oblique hypervelocity impact testing of multisheet structures, impact test results are analyzed qualitatively. In the following sections, the test data (i.e., perforation and ricochet trajectories, bumper hole dimensions) are correlated as functions of the impact parameters of the original projectile and the geometrical properties of the projectile/multisheet specimen system. These functions can be used to perform sensitivity studies and to evaluate hypothetical design configurations. A preliminary investigation of ricochet damage is performed to determine probable sizes and velocities of ricochet particles. In the final section, conclusions are made based on the analysis of the data and visual inspection of the damaged specimens. Suggestions for future experimental and analytical studies of oblique hypervelocity impact are also presented.

Experimental Procedure and Results

The oblique hypervelocity impact testing of multisheet specimens was done at the Space Debris Simulation Facility of the Materials and Processes Laboratory at the Marshall Space Flight Center. The facility consists of a light gas gun capable of launching 2.5–12.7 mm projectiles at velocities of 2–8 km/s. Projectile velocity measurements were accomplished via pulsed x-ray, laser diode detectors, and a Hall photographic station. This facility is fully described in Ref. 17. The multisheet test specimen configuration is shown in Fig. 1.

In each test, a spherical projectile of diameter d and velocity V impacted a bumper plate of thickness t_s at an angle of

obliquity θ. The projectile was shattered upon impact and created an elliptical hole in the bumper plate. Some secondary projectile and bumper plate fragments were sprayed upon the pressure wall plate a distance S away, while some fragments ricocheted and struck the ricochet witness plate. The angles θ_1 and θ_2 are "perforation angles" and denote the trajectories of the centers of mass of bumper and "in-line" projectile fragments, respectively. The angles α_c and α_{99} are "ricochet angles" and denote the trajectory of the center of mass of the ricochet fragments and the angle below which lies 99% of the damage to the ricochet witness plate, respectively.

The specimens and impact parameters were chosen to simulate the conditions of space debris impact as closely as possible and still remain within the realm of experimental feasibility. Kessler[18] states that the average mass density for pieces of orbital debris less than 10 mm in diameter is 2.8 g/cm^3, which is approximately the same as the density of aluminum. Thus, the projectiles used were solid 1100 aluminum spheres of diameter 4.75, 6.35, and 7.95 mm. Spherical projectiles were used in order to maintain consistency and repeatability. The bumper, pressure wall, and ricochet witness plates were made of 6061-T6, 2219-T87, and 2219-T6 aluminum, respectively. Their thicknesses were held constant at 1.5875, 3.175, and 2.54 mm, respectively. The angles of obliquity ranged 30 to 75 deg and the test impact velocities were 5.0–7.5 km/s. The bumper and pressure wall plates were separated by a constant distance of 101.6 mm.

A total of 22 test specimens were used to study the penetration and ricochet phenomena. The results of the test firings are presented in Table 1. The angles θ_1 and θ_2 were obtained by estimating the locations of the centers of the bumper and "in-line" projectile debris impacts on the pressure wall plates. The angle α_c was obtained by estimating the vertical location of the center of the ricochet debris impacts based on the vertical distribution of the holes, craters, etc., on the ricochet

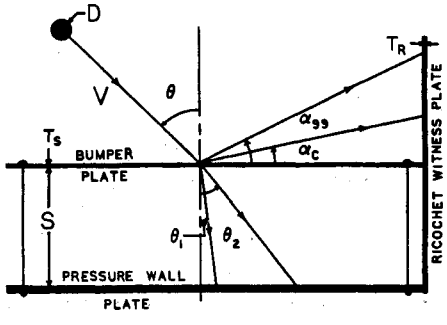

Fig. 1 Test configuration and definitions.

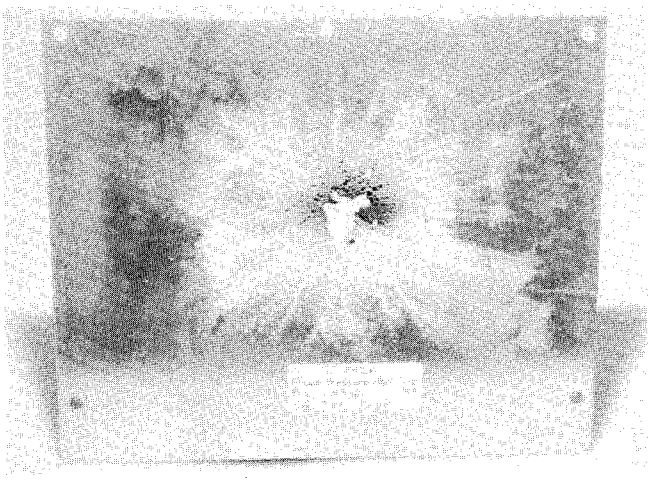

Fig. 2a 30-deg impact (EH1A)—pressure wall plate.

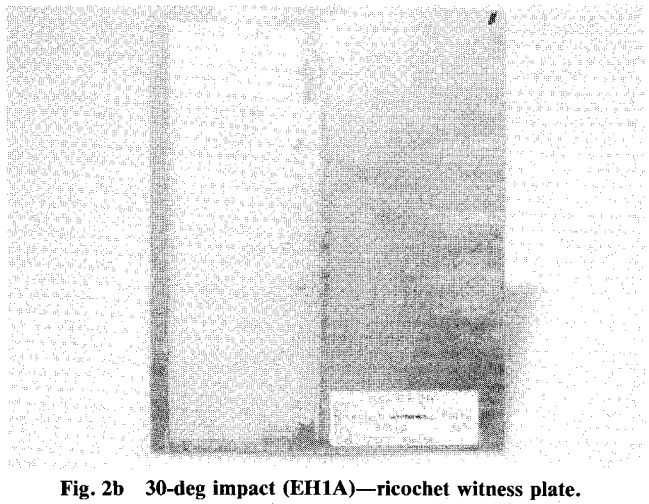

Fig. 2b 30-deg impact (EH1A)—ricochet witness plate.

Table 1 Impact test data

Test	V km/s	d mm	θ deg	D_{min} mm	D_{max} mm	Eccentricity	θ_1 deg	θ_2 deg	α_c deg	α_{99} deg
EH1A	7.07	7.95	30	16.0	17.0	1.06	—	24.8	—	—
EH1B	6.96	7.95	45	16.5	20.0	1.22	10.9	38.1	15.5	29.2
EH1C	7.14	7.95	60	16.5	24.9	1.51	9.6	50.0	11.2	27.6
EH1D	7.18	7.95	75	14.5	36.1	2.49	4.7	26.9	7.9	27.1
EHCP	7.58	4.75	75	10.0	18.0	1.82	4.7	20.9	8.2	23.6
135C	6.76	6.36	30	13.2	14.2	1.08	—	24.0	—	—
135D	6.93	6.35	30	13.2	14.2	1.08	—	27.0	—	—
136A	6.25	6.35	55	14.0	18.3	1.31	10.7	43.5	8.7	23.3
136B	7.30	6.35	55	14.0	20.1	1.44	10.1	41.8	11.9	28.3
136C	6.67	6.35	55	13.5	17.0	1.26	11.0	38.2	12.9	28.4
150A	7.08	6.35	45	14.2	18.0	1.26	10.0	39.0	11.0	24.0
157A	7.40	4.75	60	13.7	17.3	1.26	9.3	36.0	8.0	22.0
162A	6.49	4.75	30	11.9	14.0	1.18	—	21.0	—	—
162B	5.03	4.75	30	9.9	11.7	1.17	—	27.0	—	—
206F	6.24	4.75	45	11.7	13.5	1.16	8.0	31.0	8.0	21.0
208E	6.48	6.35	65	13.0	21.0	1.61	9.0	47.0	8.0	20.0
209D	7.40	6.35	65	14.5	19.6	1.36	—	—	11.0	27.0
230C	5.16	6.35	45	12.4	16.0	1.28	10.0	34.0	11.0	26.0
230D	5.59	6.35	45	13.5	16.3	1.22	10.0	37.0	10.0	25.0
230E	6.62	6.35	45	14.2	17.5	1.25	10.0	32.0	12.0	25.0
231C	6.59	7.95	65	16.5	31.0	1.87	8.7	55.7	8.4	20.4
231D	7.26	7.95	65	16.5	25.9	1.57	10.2	49.7	9.7	23.0

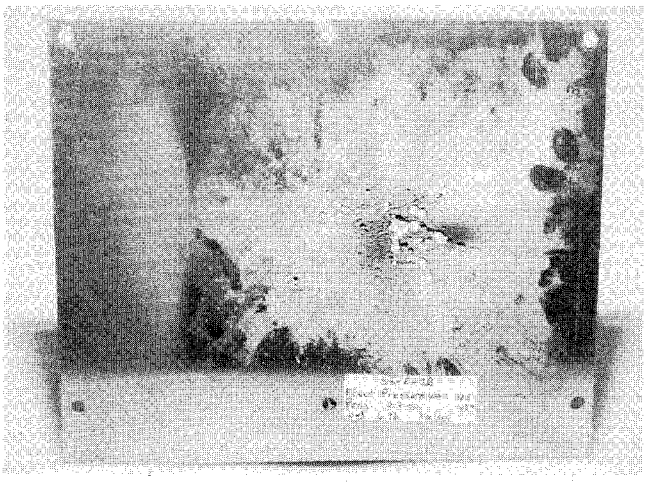

Fig. 3a 45-deg impact (EH1B)—pressure wall plate.

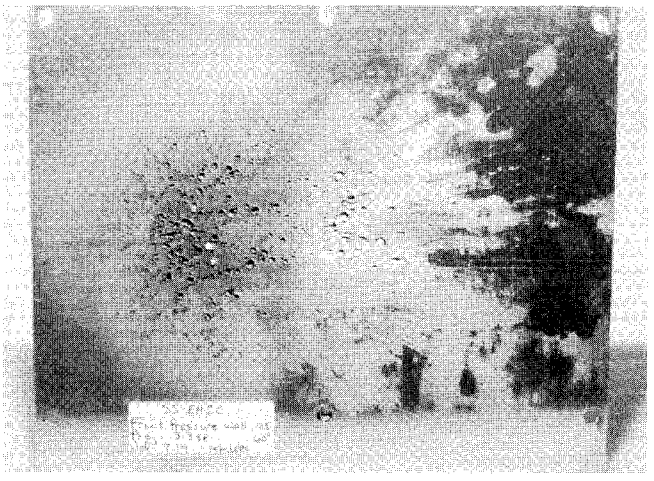

Fig. 4a 60-deg impact (EH1C)—pressure wall plate.

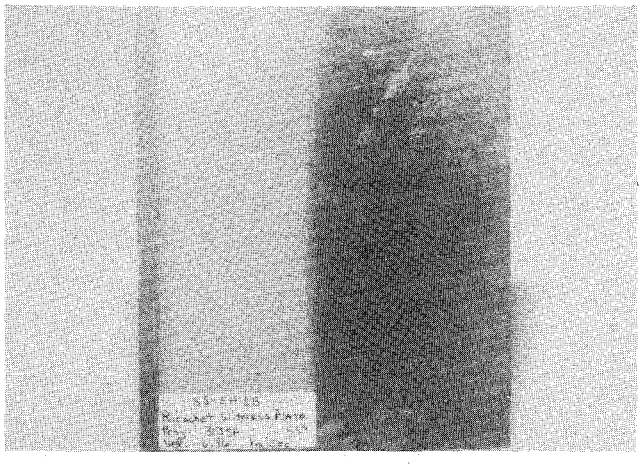

Fig. 3b 45-deg impact (EH1B)—ricochet witness plate.

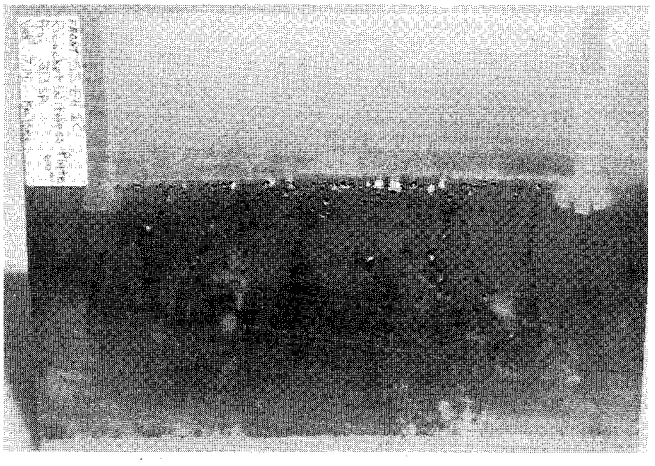

Fig. 4b 60-deg impact (EH1C)—ricochet witness plate.

witness plate. The angle α_{99} was determined based on the height below which lay 99% of the holes, craters, etc., formed by the ricochet debris. The holes and craters on the specimen plates were counted manually. Only those holes and craters 1.0 mm in diameter or greater were included in the tabulation. The minimum and maximum dimensions of the bumper plate hole, D_{min} and D_{max}, were measured directly from the bumper plate. Examples of damaged test specimens for various angles of obliquity are presented in Figs. 2–5. A more complete set of figures may be found in Ref. 19. Inspection of these and other test plates revealed several interesting features in three obliquity regimes.

Low-Obliquity Regime ($0 < \theta < 45$ deg)

For the impact tests in which the angle of obliquity was 30 deg, the bumper plate hole was elliptical with an eccentricity close to 1.0. There was extensive damage to the pressure wall plate but virtually no damage to the ricochet witness plate (Fig. 2). The pressure wall plate damage strongly resembled normal impact damage. The trajectory of the center of mass of the projectile fragments was very close to the original impact trajectory.

Medium-Obliquity Regime ($45 < \theta < 60$ deg)

The damaged pressure wall plates shown in Figs. 3a and 4a are typical of test specimens in which the trajectory obliquity of the original projectile was greater than 45 deg. Two distinct areas of damage are discernible on the plates. The damage areas on the left contain craters and holes that are nearly circular, which is characteristic of normal impact. The craters in the damage areas on the right are oblong, indicating that they were formed by oblique impacts. From these considerations, it became possible to differentiate between pressure wall plate damage caused by bumper plate fragments (circular craters and holes) and damage caused by projectile fragments (oblong craters and holes). As the trajectory obliquity of the original projectile was increased, the trajectories of the bumper plate and projectile fragments were observed to separate even more. The trajectory of the bumper fragments began to approach the normal line between the bumper and pressure wall plate while the trajectory of the projectile fragments, although no longer "in-line" with the original trajectory, was still relatively close to it. The bumper plate hole was elliptical with a steadily increasing eccentricity.

High-Obliquity Regime ($60 < \theta < 75$ deg)

With further increases in obliquity, an increasing amount of cratering and perforation was observed on the ricochet witness plates. Up to a certain critical angle, the most serious damage was still observed on the pressure wall plate, with the ricochet witness plate sustaining a relatively low level of damage (Figs. 3 and 4). However, once the critical angle was exceeded, the ricochet witness plate began to exhibit excessive cratering and perforation while the damage to the pressure wall plate decreased dramatically (Fig. 5). This critical angle is estimated to have a value between 60 and 65 deg. At obliquities beyond this critical angle, the trajectory of the shield fragments was virtually normal to the pressure wall plate and the trajectory of the projectile fragments was severely departed from the original trajectory of the impacting projectile (Fig. 5a). The bumper plate hole, although still elongated, ceased to be elliptical, becoming flattened at the end nearest to the ricochet witness

plate. This indicates that a projectile incident at a high angle of obliquity will tear, as well as shatter, the bumper plate upon impact.

Bumper Plate Hole Analysis

Elastodynamic theory predicts that as a hypervelocity projectile impacts a protective bumper plate, the projectile and the portion of the plate surrounding the impact site will break up into many fragments.[7,20] In order to be able to predict the damage potential of these fragments, it is necessary to know the volume of debris that will be produced as a result of the impact. A good estimate of the volume of bumper plate fragments can be obtained by calculating the area of the hole created during the impact. Inspection of the test specimens revealed the bumper plate hole to be elliptical with the elongation along the horizontal projection of the original projectile trajectory (see Figs. 2a, 3a, 4a, and 5a in Ref. 19). The bumper plate hole area, therefore, can be approximated as the area of an ellipse having major and minor axes equal to the maximum and minimum transverse hole dimensions, respectively. The objective of this analysis was to obtain empirical equations that relate these hole dimensions to impact parameters such as velocity, angle of obliquity, and projectile diameter.

The first task in the analysis was to determine whether existing equations that predict bumper hole diameters in normal high-speed impacts could be used to predict either dimension of the holes formed in oblique impact. A survey of the literature revealed six equations for hole diameter under normal impact (see Appendix). The equations in Ref. 21 were found to predict the minimum hole dimension under oblique impact rather well (see Table 2). However, no single equation was able to accurately predict the maximum hole dimension, even for small trajectory obliquities.

The second task undertaken was to independently derive empirical equations for the maximum and minimum hole dimensions. Inspection of the hole size data in Table 1 reveals several interesting features. First, hole dimensions can be seen to be strongly dependent on projectile diameter and impact velocity. Second, the size of the minimum dimension D_{min} appears to be relatively independent of the angle of obliquity. The maximum dimension D_{max}, however, appears to be strongly dependent on trajectory obliquity. As such, an obliquity correction term was included only in the equation for the maximum hole dimension. The equations were obtained through standard linear regression techniques with the following results:

$$\frac{D_{min}}{d} = 2.794\left(\frac{V}{C}\right)^{0.962}\left(\frac{t_s}{d}\right)^{0.895} + 1.120 \qquad 30<\theta<65 \text{ deg} \quad (1)$$

$$\frac{D_{max}}{d} = 3.841\left(\frac{V}{C}\right)^{0.415}(\sin\theta)^{1.468}\left(\frac{t_s}{d}\right)^{0.519} + 1.530 \qquad 30<\theta<75 \text{ deg} \quad (2)$$

where C is the speed of sound in the bumper plate material. The functional forms of the equations were chosen to be consistent with those in Ref. 21. The averages and standard

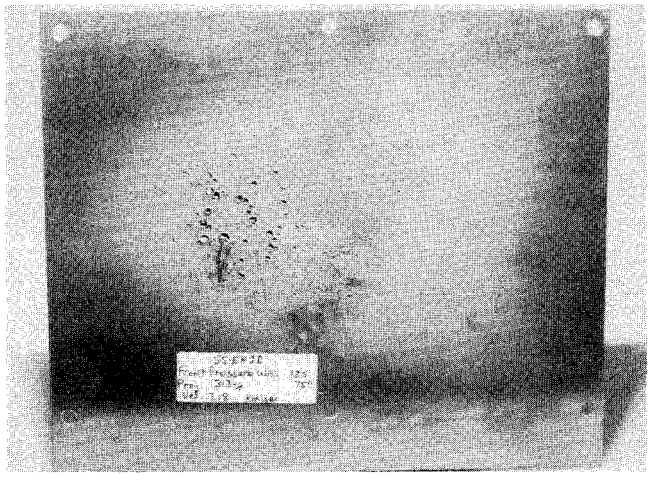

Fig. 5a 75-deg impact (EH1D)—pressure wall plate.

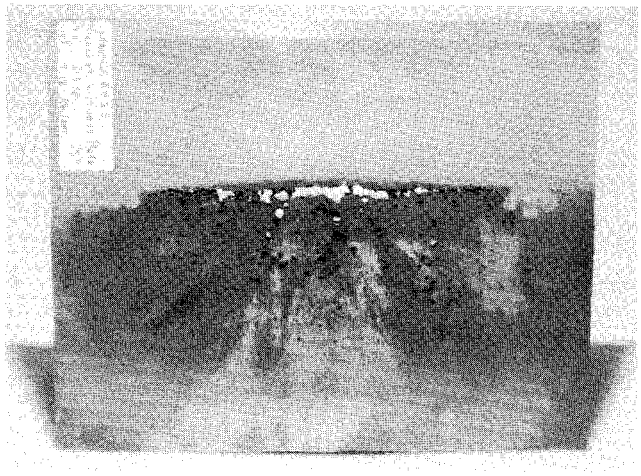

Fig. 5b 75-deg impact (EH1D)—ricochet witness plate.

Table 2 Minimum hole dimension predictions, normal impact equations

	Maiden et al.[21]		Sawle[22]	Nysmith[23]	Lundeberg et al.[24]	Rolsten et al.[25]
Equation	(A1)	(A2)	(A3)	(A4)	(A5)	(A6)
Average error, %	−4	−1	+14	−16	+7	−15
Standard deviation, %	6	6	17	5	9	14

Table 3 Regression analysis of bumper hole dimension data, error summary

Dimension	ϵ_{avg}, %	σ, %	$100R^2$
D_{min}/d	−0.001	4.016	78.7
D_{max}/d	0.002	9.821	74.3

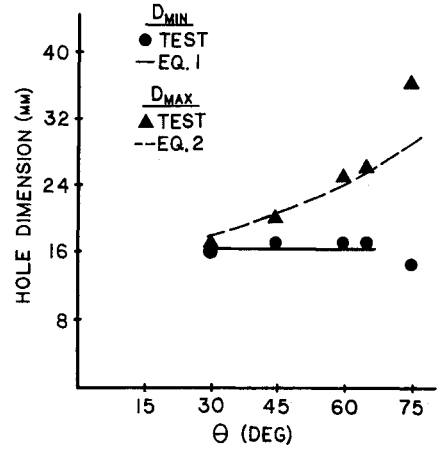

Fig. 6 Bumper plate hole dimensions—test data compared with regression equation predictions (V = 7 k/s, d = 7.95 mm).

deviations of the prediction errors of the regression equations are presented in Table 3 (columns 1 and 2, respectively). A measure of the accuracy of the regression equations, the correlation coefficient, is presented for each equation in column 3. It can be seen that the equations are a fairly good fit to the data. This is also evident in Fig. 6, which shows plots of experimental results and predicted values curves for D_{min} and D_{max} for $V = 7$ km/s. It should be noted that these equations, as well those developed in subsequent sections, are valid for aluminum projectiles and plates, and for $0.20 < t_s/d < 0.33$, and $5.0 < V < 7.6$ km/s.

Perforation Angle Analysis

Empirical expressions for θ_1 and θ_2 were obtained first as functions of the bumper plate hole dimensions and then, to be consistent with the hole size equations, as functions of projectile diameter, impact velocity, bumper plate thickness, and trajectory obliquity.

As functions of bumper hole dimensions:

$$\frac{\theta_1}{\theta} = 0.749\left(\frac{V}{C}\right)^{0.340}\left(\frac{D_{min}}{d}\right)^{0.197}\left(\frac{D_{max}}{d}\right)^{-1.504}$$

$45 < \theta < 60$ deg (3a)

$$\frac{\theta_1}{\theta} = 7.359\left(\frac{V}{C}\right)^{-3.221}\left(\frac{D_{min}}{d}\right)^{-0.296}\left(\frac{D_{max}}{d}\right)^{-2.279}$$

$65 < \theta < 75$ deg (3b)

$$\frac{\theta_2}{\theta} = 1.566\left(\frac{V}{C}\right)^{0.581}\left(\frac{D_{min}}{d}\right)^{-0.784}\left(\frac{D_{max}}{d}\right)^{-0.128}$$

$30 < \theta < 60$ deg (4a)

Table 4 Regression analysis of penetration angle data, error summary

As functions of	Impact angle, deg	ϵ_{avg},%	σ,%	$100R^2$
Hole dimensions, θ_1/θ	$45 < \theta < 60$	0.198	6.707	80.2
	$65 < \theta < 75$	1.751	21.050	78.9
Impact parameters, θ_1/θ	$45 < \theta < 60$	0.207	6.903	79.5
	$65 < \theta < 75$	0.028	2.678	99.7
Hole dimensions, θ_2/θ	$30 < \theta < 60$	0.251	7.353	57.8
	$65 < \theta < 75$	2.921	27.303	71.6
Impact parameters, θ_2/θ	$30 < \theta < 60$	0.254	7.314	56.8
	$65 < \theta < 75$	0.032	2.822	99.7

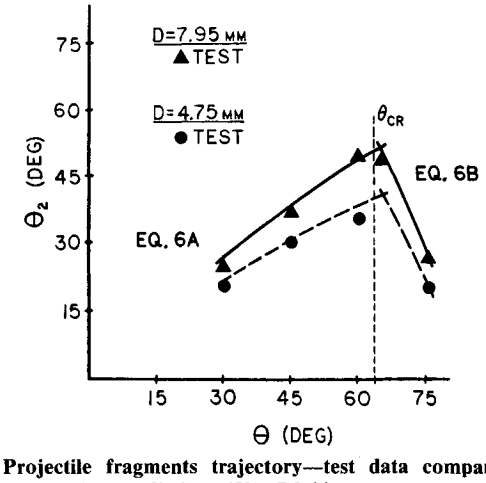

Fig. 7 Projectile fragments trajectory—test data compared with regression equation predictions ($V = 7$ k/s).

$$\frac{\theta_2}{\theta} = 24.444\left(\frac{V}{C}\right)^{-4.935}\left(\frac{D_{min}}{d}\right)^{-0.137}\left(\frac{D_{max}}{d}\right)^{-1.584}$$

$65 < \theta < 75$ deg (4b)

As functions of original impact parameters:

$$\frac{\theta_1}{\theta} = 0.089\left(\frac{V}{C}\right)^{-0.082}(\sin\theta)^{-1.227}\left(\frac{t_s}{d}\right)^{-0.362}$$

$45 < \theta < 60$ deg (5a)

$$\frac{\theta_1}{\theta} = 0.023\left(\frac{V}{C}\right)^{1.109}(\sin\theta)^{-14.223}\left(\frac{t_s}{d}\right)^{-0.069}$$

$65 < \theta < 75$ deg (5b)

$$\frac{\theta_2}{\theta} = 0.436\left(\frac{V}{C}\right)^{-0.296}(\sin\theta)^{-0.233}\left(\frac{t_s}{d}\right)^{-0.415}$$

$30 < \theta < 60$ deg (6a)

$$\frac{\theta_2}{\theta} = 0.138\left(\frac{V}{C}\right)^{-0.606}(\sin\theta)^{-11.979}\left(\frac{t_s}{d}\right)^{-0.477}$$

$65 < \theta < 75$ deg (6b)

The averages and standard deviations of the prediction errors and the correlation coefficients are presented in Table 4. Inspection of the correlation coefficients reveals that the θ_2 data did not regress as well as the θ_1 data. This is in part due to the difficulty in determining the exact locations on the pressure wall plate of the centers of mass of the particle sprays. Furthermore, the "in-line" trajectory angle θ_2 is not a single-valued function of trajectory obliquity θ. It can be seen in Fig. 7 that θ_2 varies directly with θ up to a critical value θ_{cr} between 60 and 65 deg and then decreases with further increases in θ. This reversal at $\theta = \theta_{cr}$ corresponds to a change in the location of the most severe damage from the pressure wall plate for $\theta < \theta_{cr}$ to the ricochet witness plate for $\theta > \theta_{cr}$.

Ricochet Angle Analysis

Empirical expressions for α_c and α_{99} were obtained first as functions of the bumper plate hole dimensions and then as functions of projectile diameter, impact velocity, bumper plate thickness, and trajectory obliquity.

As functions of bumper hole dimensions:

$$\frac{\alpha_c}{\theta} = 2.138\left(\frac{V}{C}\right)^{0.926}\left(\frac{D_{min}}{d}\right)^{-0.453}\left(\frac{D_{max}}{d}\right)^{-2.119}$$

$45 < \theta < 75$ deg (7)

$$\frac{\alpha_{99}}{\theta} = 2.163\left(\frac{V}{C}\right)^{0.335}\left(\frac{D_{min}}{d}\right)^{-0.266}\left(\frac{D_{max}}{d}\right)^{-1.310}$$

$45 < \theta < 75$ deg (8)

As functions of original impact parameters:

$$\frac{\alpha_c}{\theta} = 0.036\left(\frac{V}{C}\right)^{0.909}(\sin\theta)^{-2.959}\left(\frac{t_s}{d}\right)^{-0.536}$$

$45 < \theta < 75$ deg (9)

$$\frac{\alpha_{99}}{\theta} = 0.177\left(\frac{V}{C}\right)^{0.434}(\sin\theta)^{-1.985}\left(\frac{t_s}{d}\right)^{-0.278}$$

$45 < \theta < 75$ deg (10)

Average prediction errors, standard deviations, and correlation coefficients are presented in Table 5. It can be seen that,

although the average prediction errors are quite small, the spread of the errors is somewhat large for these equations. This is due to error in the regression data itself, which can be attributed to several factors. First, the ricochet witness plates were finite in height. Some ricochet debris particles escaped detection and, therefore, were not included in the final tally. Second, ricochet debris holes and craters were frequently observed to cluster and overlap, especially for large values of original trajectory obliquity. In these cases it was difficult to determine the exact number of holes or craters on the ricochet witness plate. The total number of ricochet debris craters and holes therefore is seen somewhat dependent on the person performing the analysis. Plots of α_c and α_{99} as functions of θ for $V = 7$ km/s are shown in Fig. 8. Once again, these equations are valid for aluminum projectiles and plates. Since no ricochet damage was observed for obliquities below 45 deg, these equations are valid only for $45 < \theta < 75$ deg.

Ricochet Particle Size and Velocity Analysis

The next step in the analysis of the oblique impact test specimens was to determine the sizes and velocities of ricochet debris particles using the crater and hole damage on the ricochet witness plates. The following observations were made during inspection of ricochet witness plate damage:

1) Crater dimensions, such as diameter and depth, were found to increase with increasing trajectory obliquity. Penetration depths were observed to decrease with increasing projectile diameter and to increase with increasing original impact velocity.

2) The craters and holes were approximately circular in shape with very little elongation. This is not very surprising since the α_{99} data in Table 1 indicates that 99% of the ricochet impacts occurred within angles of 30 deg with respect to the plane of the bumper plate.

3) Hole diameters were found to increase with increasing trajectory obliquity and with increasing projectile diameter.

4) The ricochet plates exhibited an excessive amount of dimpling, spalling, and perforation, especially at larger angles of obliquity and higher impact velocities. This damage was concentrated within an angle of 15 deg with respect to the plane of the bumper plate.

Examination of existing hole and crater depth diameter equations revealed a strong coupling between particle size and velocity effects. That is, the same size hole can be produced by a small particle traveling at a high speed or by a larger particle traveling at a slower speed. This ambiguity makes exact calculation of ricochet particle sizes and speeds extremely difficult.

However, it was possible to estimate a range of probable ricochet velocities based on an assumed range of probable particle diameters. These velocities were calculated by using the normal impact equations for hole diameters to solve for velocity in terms of all the other quantities. The lower limit of the particle diameter range was set by the limit of applicability of the equations. In most cases, this value was equal to 1.25 mm. For the purposes of this investigation, the upper limit on the particle size was assumed to be equal to one-half of the original projectile diameter. Substitution of appropriate parameters led to the conclusion that ricochet velocities can exceed 10 km/s for the smaller particles but can be as low as 0.5 km/s for the larger particles. Thus, there is a good probability that some of the the larger ricochet debris particles travel at low velocities. These large low-speed particles can be expected to inflict more serious damage than the smaller ones traveling at higher velocities.[7] In order to understand this phenomenon more fully, further tests will have to be made in which little or no perforation of the ricochet witness plate is allowed to occur. Under these conditions, ballistic limit equations, as well as penetration depth equations, can be used to obtain better estimates of ricochet particle sizes and velocities.

Table 5 Regression analysis of ricochet angle data, error summary

As functions of	Ricochet angle	ϵ_{avg},%	σ,%	$100R^2$
Hole dimensions	α_c/θ	0.989	14.742	82.0
	α_{99}/θ	0.783	13.208	71.2
Impact parameters	α_c/θ	0.851	13.389	84.2
	α_{99}/θ	0.501	10.406	81.3

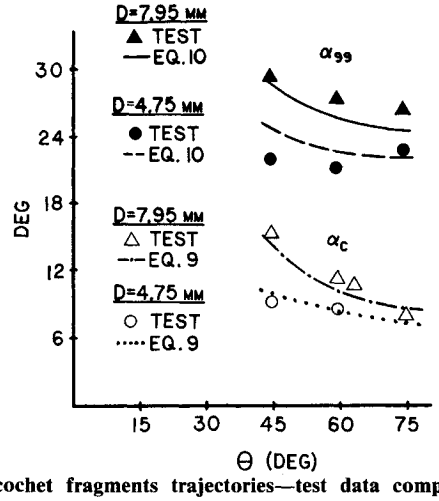

Fig. 8 Ricochet fragments trajectories—test data compared with regression equation predictions ($V = 7$ k/s).

Conclusions and Recommendations

An investigation of oblique hypervelocity impact has been successfully completed. Several conclusions can be drawn from the analysis of key components in the problem of oblique hypervelocity impact on multisheet specimens. These conclusions can have a wide range of consequences on the design of spacecraft meteoroid and space debris protection systems.

1) There exists a critical angle of obliquity. Projectiles with angles of obliquity less than this critical angle produce significant damage to the interior pressure wall and little damage to the ricochet witness plate. Projectiles with trajectory obliquities greater than the critical angle produce little damage to the pressure wall plate but produce ricochet debris that causes major damage to the ricochet witness plate. This critical angle is estimated to have a value between 60 and 65 deg. The existence of such an angle has serious implications for the design and placement of external subsystems on spacecraft that are developed for long-duration missions in the meteoroid and space debris environment. In order to determine a more precise value of this critical angle, a more sophisticated damage criterion is needed. It also should be determined if the critical angle is dependent on any material, geometric, or impact parameters.

2) The damage potential of ricochet debris is difficult to extrapolate from existing damage data due to coupling effects of ricochet particle size and velocity. Initial investigations reveal that the velocities of small ricochet debris particles can exceed the original projectile impact velocity, whereas the velocities of larger particles can enter the dangerous low velocity regime. Damage produced by the larger, slower particles was found to be more serious than that produced by the smaller, faster particles.

3) The most serious ricochet damage was found to occur within an angle of 15 deg with respect to the plane of the bumper plate regardless of the original angle of impact. For original trajectory obliquities of greater than 60 deg, the ricochet plate was completely perforated at the bumper plate/ricochet witness plate interface. In general, ricochet damage was found to increase with increases in original projectile obliquity, impact velocity, and size. A preliminary investiga-

tion of the angles at which the ricochet particles that create the largest hole or deepest crater strike the witness plate was performed, but the results were inconclusive. Knowledge of these angles would enable a designer to estimate critical exterior locations and avoid them in the placement of exterior subsystem components.

4) Additional experimental studies are needed in order to be able to more accurately assess the extent of ricochet damage due to an oblique hypervelocity impact. Such investigations would result in more reliable design methodologies for meteoroid and space debris protection systems for long-duration spacecraft. Future testing of oblique impact testing should be conducted with ricochet witness plates sufficiently thick so that little or no spalling or perforation occurs. In this manner, virtually all the crater damage produced by ricochet particles can be used with thick plate equations to estimate ricochet velocities and particle sizes. Future experimental investigations also should be conducted with projectiles and specimen plates made from different materials. The testing then will better simulate on-orbit impacts of meteoroids or pieces of space debris with spacecraft materials. Use of a wide variety of materials, including composites, will also serve to improve and expand the applicability of the current empirical expressions.

5) Extensive analytical investigations of the phenomena involved in oblique hypervelocity impact are strongly recommended. Such investigations would achieve several important goals. First, they would provide verification of the empirical model developed in this study. Second, they would provide reliable means of predicting ricochet damage through accurate estimates of ricochet particle sizes and velocities. Third, they would yield damage criteria that would be applicable in a variety of impact situations.

Appendix: Thin-Plate Hole Diameter Equations, Normal Hypervelocity Projectile Impact

From Ref. 21:

$$D/d = 0.45V(t_s/d)^{0.666} + 0.90$$

$$1.0 < D/d < 3.5,\ 0.040 < t_s/d < 0.504$$

$$1.0 < V < 8.0 \text{ km/s} \quad \text{(A1)}$$

From Ref. 21:

$$D/d = 2.40(V/C)(t_s/d)^{0.666} + 0.90$$

$$1.0 < D/d < 3.5,\ 0.040 < t_s/d < 0.504$$

$$1.0 < V < 8.0 \text{ km/s} \quad \text{(A2)}$$

From Ref. 22:

$$D/d = 3.2[(\rho_p/\rho_t)(V/C)^{0.222}(t_s/d)^{0.666} + 1.0$$

$$0.8 < D/d < 3.66,\ 0.083 < t_s/d < 0.333$$

$$11.0 < V < 17.0 \text{ km/s} \quad \text{(A3)}$$

From Ref. 23:

$$D/d = 1.32(t_s/d)^{0.45}V^{0.50}$$

$$1.5 < D/d < 3.75,\ 0.25 < t_s/d < 1.00$$

$$3.2 < V < 8.8 \text{ km/s} \quad \text{(A4)}$$

From Ref. 24:

$$D/d = 3.4(t_s/d)^{0.333}(V/C)^{0.333}(1.0 - 0.0308\rho_t/\rho_p)$$

$$1.0 < D/d < 4.5,\ 0.5 < t_s/d < 125$$

$$4.5 < V < 8.2 \text{ km/s} \quad \text{(A5)}$$

From Ref. 25:

$$D/d = [2.0 + (\rho_p/\rho_t)^{0.5}]^{0.5}$$

$$1.4 < D/d < 2.2,\ 0.040 < t_s/d < 0.748$$

$$2.3 < V < 4.9 \text{ km/s} \quad \text{(A6)}$$

where D is the hole diameter and ρ_p and ρ_t the projectile, bumper plate material density, respectively.

Acknowledgments

The authors are grateful for the support of the NASA/ASEE Summer Faculty Fellowship Program. The authors also wish to express their appreciation to Hubert Smith and Joe Lambert of the Laboratory Support Branch of the Materials and Processes Laboratory, Phillip Petty and Robert Stowell of Martin Marietta Corporation, and Ben Ramsey and Earl Shirley of the Boeing Corporation for conducting the simulation impact testing that made this report possible. The authors are also grateful to Maher Almoghraby for assistance in the computer programming.

References

[1]Kessler, D. J. and Cour-Palais, B. G., "Collision Frequency of Artificial Satellites: The Creation of a Debris Belt," *Journal of Geophysical Research,* Vol. 83, June 1978, pp. 2637–2646.

[2]Kessler, D. J., "Sources of Orbital Debris and the Projected Environment for Future Spacecraft," *Journal of Spacecraft,* Vol. 18. July–August 1981, pp. 357–360.

[3]Reynolds, R. C., Fisher, N. H. and Rice, E. E., "Man-Made Debris in Low Earth Orbit—A Threat to Future Space Operations," *Journal of Spacecraft,* Vol. 20, May–June 1983, pp. 279–285.

[4]Kessler, D. J., and Su, S. Y., *Orbital Debris,* NASA CP-2360, March 1985.

[5]Whipple, E. L., "Meteorites and Space Travel," *Astronomical Journal,* Vol. 52, March 1947, p. 5.

[6]Wallace, R. R., Vinson, J. R. and Kornhauser, M., "Effects of Hypervelocity Particles on Shielded Structures," *ARS Journal,* Vol. 32, Aug. 1962, pp. 1231–1237.

[7]Maiden, C. J. and McMillan, A. R., "An Investigation of the Protection Afforded a Spacecraft by a Thin Shield," *AIAA Journal,* Vol. 2, Nov. 1964, pp. 1992–1998.

[8]Lundeberg, J. F., Lee, D. H., and Burch, G. T., "Impact Penetration of Manned Spacecraft," *Journal of Spacecraft,* Vol. 3, Feb. 1966, pp. 182–187.

[9]Riney, T. D. and Halda, E. J., "Effectiveness of Meteoroid Bumpers Composed of Two Layers of Distinct Materials," *AIAA Journal,* Vol. 6, Feb. 1968, pp. 338–344.

[10]Wilkinson, J. P. D., "A Penetration Criterion for Double-Walled Structures Subject to Meteoroid Impact," *AIAA Journal,* Vol. 7, Oct. 1969, pp. 1937–1943.

[11]Swift, H. F., Bamford, R., and Chen, R., "Designing Space Vehicle Shields for Meteoroid Protection: A New Analysis," *Advances in Space Research,* Vol. 2, No. 12, 1983, pp. 219–234.

[12]Coronado, A. R., Gibbins, M. N., Wright, M. A., and Stern, P. H., "Space Station Integrated Wall Design and Penetration Damage Control," Boeing Aerospace Company, Seattle, WA, Rept. D180-30550-1, July 1987.

[13]Summers, J. L., "Investigation of High Speed Impact: Regions of Impact and Impact at Oblique Angles," NASA TN D-94, Oct. 1959.

[14]Burch. G. T., "Multi-plate Damage Study," U.S. Air Force Armament Lab., Eglin AFB, FL, AF-ATL-TR-67-116, Sept. 1967.

[15]McMillan, A. R., "Experimental Investigations of Simulated Meteoroid Damage to Various Spacecraft Structures," NASA CR-915, Jan. 1968.

[16]Merzhievskii, L., and Urushkin. V., "Oblique Collision of a High-Speed Particle with a Shield ," *Combustion, Explosions, and Shock Waves,* Vol. 16, March 1981, pp. 551-555. (translation).
[17]Taylor, R. A., "A Space Debris Simulation Facility for Spacecraft Materials Evaluation," *SAMPE Quarterly,* Vol. 18, Feb. 1987, pp. 28-34.
[18]Kessler, D. J., "Orbital Debris Environment for Space Station," NASA JSC Doc. 20001, 1984.
[19]Schonberg, W. P., Taylor, R. A., and Horn, J. R., "An Analysis of Penetration and Ricochet Phenomena in Oblique Hypervelocity Impact," NASA TM-100319, Feb. 1988.
[20]Cour-Palais, B. G., "Space Vehicle Meteoroid Shielding Design," *Proceedings of the Comet Halley Micrometeoroid Hazard Workshop,* European Space Agence, Paris, SP-153, 1979, pp. 85-92.
[21]Maiden, C. J., Gehring, J. W., and McMillan, A. R., "Investigation of Fundamental Mechanism of Damage to Thin Targets by Hypervelocity Projectiles," General Motors Defense Research Laboratory, Santa Barbara, CA, GM-DRL-TR-63-225, Sept. 1963.
[22]Sawle, D. R., "Hypervelocity Impact on Thin Sheets and Semi-Infinite Targets at 15 km/sec,"*AIAA Journal,* Vol. 8, July 1970, pp. 1240-1244.
[23]Nysmith, C. R., "Penetration Resistance of Double Sheet Structures at Velocities to 8. 8 km/sec," NASA TN-D-4568, May 1968.
[24]Lundeberg, J. F., Stern, P. H., and Bristow, R. J., "Meteoroid Protection for Spacecraft Structures," NASA CR-54201, Oct. 1965.
[25]Rolsten, R. F., Wellnitz, J. N., and Hunt, H. H., "An Example of Hole Diameter in Thin Plates Due to Hypervelocity Impact," *Journal of Applied Physics,* Vol. 33, March 1964, p. 556-559.